



Design and performance of a high-speed and low-noise preamplifier for SiPM*

Xi-Yang Wang,¹ Hong-Yu Zhang ¹, De-Qing Fang,¹ Wan-Bing He,^{1,2} Xiao-Long Wang ^{1,†}, Qi-Bin Zheng,³ and Shi-Ming Zou¹

¹Key Laboratory of Nuclear Physics and Ion-beam Application (MOE) and Institute of Modern Physics, Fudan University, Shanghai 200433, China

²Shanghai Research Center for Theoretical Nuclear Physics, NSFC and Fudan University, Shanghai 200438, China

³Laboratory of Radiation Detection and Medical Imaging and School of Health Science and Engineering, University of Shanghai for Science and Technology, Shanghai 200093, China

Considering the R&D for upgrading the K_L^0 and μ detectors in the Belle II experiment using a scintillator and silicon photomultiplier (SiPM), we designed a compact high-speed and low-noise preamplifier. The preamplifier demonstrated a good gain stability, bandwidth of 426 MHz, baseline noise level of $\sigma \approx 0.6$ mV, dynamic range of up to 170 mV of the input signal amplitude, good time resolution of 20 ps, and it can be comprehensively applied to SiPMs. Adopting pole-zero-cancellation in the preamplifier reduces both the rise and fall times of the SiPM signal, which can significantly improve the time resolution and reduce the pile-up when using a large SiPM or an array of SiPMs. Various combinations of the preamplifier and several types of SiPMs demonstrated time resolutions better than 50 ps for most cases; when the number of detected photons was larger than 60, a time resolution of approximately 25 ps was achieved.

Keywords: Silicon photomultiplier, High-speed amplifier, Low noise, High time resolution

I. INTRODUCTION

Detector technology with scintillation has been utilized in experiments for a long time, such as the ZnS in the Rutherford experiment. This technology is being rapidly developed, especially considering the various inorganic scintillators, such as BGO, PWO, and LYSO, among others, as well as the new photon detector based on silicon [1, 2]. Detecting technologies with scintillation and photomultipliers are comprehensively used in experiments for particle and nuclear physics. The Belle II experiment [3, 4], which is a super B factory and started its physics run in 2019, uses various photon detection technologies such as the time-of-propagation counter and the Aerogel ring-imaging Cherenkov detector for charged particle identification, the electromagnetic calorimeter for high energy photon detection, and the K_L^0 and muon detector (KLM) for identifications of K_L^0 and muon [5]. The KLM detector modules in the endcaps and the two inner-most layers of the barrel are based on a combination of an extruded scintillator and a wavelength-shifting fiber and silicon photomultiplier (SiPM), in contrast to the resistive plate chambers (RPCs) used in the Belle KLM. The new technology has demonstrated a good performance; however, the remaining 13 layers of the barrel KLM are still using the legacy RPCs from the Belle. As indicated in the Snowmass Whitepaper [6], Belle II is considering upgrading the KLM with all scintillator modules, which contain approximately 38,000 readout channels. By utilizing the advantage of good timing from the scintillator and SiPM, it is possible to measure the time-of-flight of

neutral hadrons, such as K_L^0 and the neutron. This is critical for improving the K_L^0 identification and furthermore, for measuring the momentum of K_L^0 or the neutron. Meanwhile, the scheme of using the SiPM and plastic scintillation system to build a muon detector or a hadron calorimeter is also expected to be used in the proposed Circular Electron Positron Collider (CEPC), which is a Higgs factory. [7, 8]

The SiPM is a novel photodetector composed of parallel avalanche diodes that operate in the Geiger mode. It has several advantages, such as its small size, low operation voltage (V_{op}), excellent time resolution, and resistance to magnetic field interference. The SiPM is commonly used for scientific research, medical diagnosis, and biochemical detection [9–12]. The rise-time (τ_{rise}) of a signal from the SiPM is only within hundreds of pico-seconds; therefore, photon detection with SiPM can achieve a very good timing performance with an excellent front-end readout. A signal from the SiPM is always small and needs to be amplified at the front-end, and the timing performance is mainly constrained by the bandwidth and the noise level of the amplifier; this front-end readout is called a preamplifier. Furthermore, as the photosensitive area of the SiPM increases, its dark counting rate significantly increases and becomes an issue for the design of the preamplifier. In practice, detectors in particle and nuclear physics experiments usually need to place hundreds or thousands of channels of front-end readout electronics in a small space. Thus, the preamplifier must be low-cost and compact for multi-channel integration. Certain commercial preamplifiers for SiPM are available [13–15]; however, they typically have large volumes, complex circuits, and it is difficult to match the requirements of a high time resolution and high integration in a large-scale detector.

Considering the R&D for the KLM upgrade in Belle II and the muon detector in CEPC, we designed a compact preamplifier that operates for various SiPMs. This preamplifier has the advantages of a fast rise time, low noise level, low cost, and

* This work was partially supported by the National Key R&D Program of China (No. 2022YFA1601903), the National Natural Science Foundation of China (Nos. 11925502, 11961141003, and 12175041), and the Strategic Priority Research Program of the CAS (No. XDB34030000).

† Corresponding author, xiaolong@fudan.edu.cn

simple circuit form. In this study, we introduce the design and performance of this preamplifier, followed by the time resolution obtained from the combinations of the preamplifier and different types of SiPMs.

II. DESIGN OF THE PREAMPLIFIER

Figure 1(a) presents the circuit diagram of a SiPM equivalent model [16–18], where C_d , R_d , and R_q indicate the capacitance of the reverse-biased diode, resistance of the diode, and resistance of the quenching resistor; C_q is the parasitic capacitance of R_q , and R_s is the load resistance of SiPM. When the SiPM operating at V_{op} , $Q = (C_d + C_q)(V_{op} - V_{br})$ is related to its gain, V_{br} is its breakdown voltage. For a SiPM containing N_{pixel} pixels, the total capacitance is $C_{tot} = N_{pixel} \cdot (C_d + C_q)$. Figure 1(b) demonstrates the LTspice simulation [19] with parameters of S13360-6025PE [20] for a typical SiPM signal, which has a fast rise time $\tau_{rise} = R_d(C_d + C_q)$ and slow fall time τ_{fall} that can be described as follows:

$$i_d(t) = \frac{QR_s}{C_q + C_d} \cdot \left(\frac{C_q}{\tau_{fall}^{fast}} e^{\frac{-t}{\tau_{fall}^{fast}}} - \frac{C_d}{\tau_{fall}^{slow}} e^{\frac{-t}{\tau_{fall}^{slow}}} \right), \quad (1)$$

where $\tau_{fall}^{fast} = R_s C_{tot}$ and $\tau_{fall}^{slow} = R_q(C_d + C_q)$ are the fast and slow components of τ_{fall} , respectively. When multiple SiPMs are combined in parallel for a large total photosensitive area, both τ_{rise} and τ_{fall} increase [21]. A large τ_{rise} is a disadvantage for a good time resolution, and a large τ_{fall} usually causes pile-up in fetching a signal and increases the dead time of a detector. This is problematic for an ultra-high luminosity experiment such as Belle II, which was designed for a luminosity of $0.8 \times 10^{36} \text{ cm}^{-2}\text{s}^{-1}$. To reduce the long τ_{fall} , we can use the pole zero cancellation (PZC) in the preamplifier; the τ_{rise} is also reduced by PZC.

Considering the requirements of a large bandwidth and low noise level, the operational amplifier chip LMH6629 from TI Company [22] was chosen to design the preamplifier. This chip has a voltage slew rate of $1600 \text{ V}/\mu\text{s}$, an input voltage noise of $0.69 \text{ nV}/\sqrt{\text{Hz}}$, and a -3dB bandwidth of 900 MHz at a stable gain of $+10 \text{ V/V}$. LMH6629 is sufficient for a significantly fast τ_{rise} of the SiPM signal.

Figure 2(b) presents the principle diagram of the preamplifier circuit. It adopts the form of negative feedback to improve the τ_{rise} of the output signal and the stability of the gain. For applications with multiple channels in the experiment, a power supply board for 8-channel parallel preamplifiers was designed, as shown in Fig. 2(c). The preamplifier units are directly inserted into the power supply board and connected to the SiPM readout boards through RF cables. This design can match different sizes of readout boards and various types of SiPMs, which increases the versatility of the preamplifier.

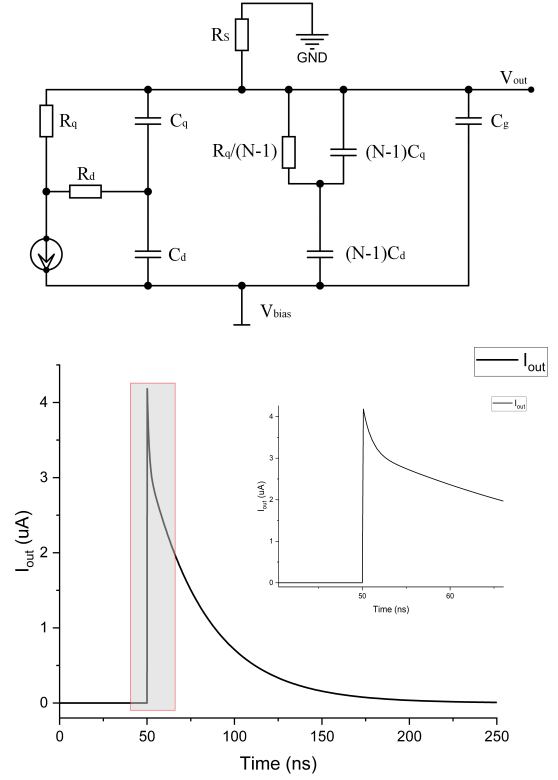


Fig. 1. Circuit diagram of the SiPM equivalent model [16] and output signal from the SiPM. The left plot demonstrates the equivalent model whereas the right plot presents the LTspice simulation with parameters of S13360-6025PE [20] for a typical SiPM signal, which consists of a fast rising edge and falling edge containing a fast component and a slow component.

A. Bandwidth and noise

The effect of electronic noise on the systematic timing performance is estimated by the following [23]:

$$\sigma_t = \frac{\sigma_{noise}}{dV/dt}, \quad (2)$$

where σ_{noise} is the baseline noise level, and dV/dt is the voltage slope of the rising edge of the signal. To achieve a τ_{rise} of approximately 1 ns , the bandwidth of the amplifier (f_{BW}) should be approximately $f_{BW} = 0.35/\tau_{rise} = 350 \text{ MHz}$. Thus, we set the amplifier gain to 26dB with $R_f = 1 \text{ k}\Omega$ and $R_g = 50 \Omega$ for the negative feedback, as shown in Fig. 2(a). According to the data manual of LMH6629 [22], we calculated the bandwidth of the preamplifier to be 428 MHz . With a normal load resistance $R_s = 50 \Omega$, the preamplifier has a current gain of 1050 V/A for the current signal output from the SiPM.

The equivalent noise at the input of the preamplifier can be calculated according to Ref. [22] as follows:

$$e_{ni} = \sqrt{e_n^2 + (i_n R_s)^2 + 4kTR_s + [i_n(R_f || R_g)]^2 + 4kT(R_f || R_g)}, \quad (3)$$

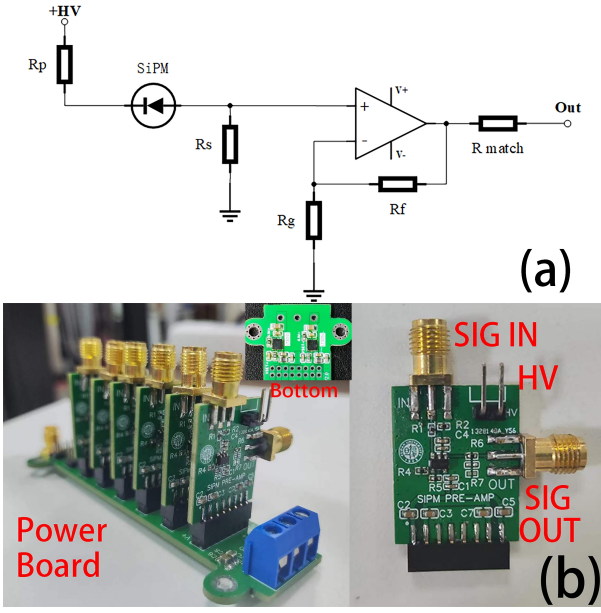


Fig. 2. (Color online) The compact preamplifier designed for a high time resolution. Plot (a) presents the schematic diagram of the preamplifier, and plot (b) presents an image of the bunch of 8-channel preamplifiers with a common power supply board. The ‘SIG IN’ connector is for the input signal from SiPM, and the ‘SIG OUT’ connector is for the output signal being amplified. The ‘HV’ pins are for the V_{op} for the SiPM operation. The inserted image in (b) presents the regulators at the bottom of the power supply board.

where e_n and i_n are the intrinsic input voltage noise and intrinsic current noise; k and T are the Boltzman constant and temperature, respectively. LMH6629 is an ultra-low noise operational amplifier with $e_n = 0.69 \text{ nV}/\sqrt{\text{Hz}}$ and $i_n = 2.6 \text{ pA}/\sqrt{\text{Hz}}$. We calculated the equivalent noise to be $e_{ni} = 1.41 \text{ nV}/\sqrt{\text{Hz}}$. By integrating e_{ni} in the bandwidth, the noise level of the preamplifier baseline is $\sigma_{\text{noise}} \sim 587 \mu\text{V}$. Here, as well as hereafter, σ of the Gaussian function is used for a time resolution or a noise level. Via a simulation with LTspice [19], a -3 dB bandwidth of 417 MHz and noise level of $\sigma_{\text{noise}} \approx 517 \mu\text{V}$ were obtained, which are consistent with the calculations. We also used the N5222B network analyzer to measure the frequency characteristics of the preamplifier ranging between 10 MHz – 1 GHz , and obtained a -3 dB bandwidth of 426 MHz for small signals with 200 mVpp or 240 MHz for large signals with 2 Vpp .

In reality, to suppress the noise from the power supply and increase the reliability of the amplifier, we designed a four-layer structure PCB and placed all the components around the LMH6629 to shorten the connection. We also used the super-high power supply rejection ratio (PSRR), ultra-low noise positive regulator LT3045, and negative regulator LT3094 to reduce the ripple from the power supply, as shown in the inserted image in Fig. 2(b).

B. PZC to reduce the pile-up

According to Eq. (1), the fast component of the falling edge $\tau_{\text{fall}}^{\text{fast}}$ is mainly determined by the load resistance R_s . For certain SiPMs that have a high gain and are large, such as the Hamamatsu MPPC S13360-6025PE [24], the terminal capacitance C_{tot} is 1280 pF . If $R_s = 50 \Omega$, the $\tau_{\text{fall}}^{\text{fast}}$ is approximately 64 ns and the total τ_{fall} is significantly longer, which may lead to the pile-up in a detector using SiPM.

Adding a PZC in the circuit of a preamplifier is a sufficient method for reducing the τ_{fall} and avoiding the signal pile-up by attenuating the low-frequency components in the output signal. The PZC also reduces the τ_{rise} , which is useful for increasing the time resolution of the preamplifier according to Eq. (2). Figure 3(a) presents the implementation of the PZC in the preamplifier. The transfer function of the PZC in the frequency domain can be described as follows:

$$V_0(s) = \frac{s + \tau_1^{-1}}{(s + \tau_f^{-1})(s + \tau_2^{-1})} \cdot V_{\text{max}}, \quad (4)$$

where V_{max} is the maximum amplitude of the output signal from the preamplifier, $\tau_f = R_q C_d$, $\tau_1 = R_1 C_1$, and $\tau_2 = R_1 R_2 C_1 / (R_1 + R_2)$. The signal reaches zero cancellation when $\tau_1 = \tau_f$, thus the attenuation time of the output signal changes to τ_2 ($\tau_2 < \tau_1$).

The LTspice simulation demonstrates that the output impedance after the PZC network is no longer a constant 50Ω and the signal amplitude is reduced. To compensate for the gain lost and ensure an output impedance of 50Ω , we can use a two-stage amplifier after the PZC, as shown in Fig. 3(a). To demonstrate the effect of PZC on the signal shape, we used DT5810B [25] to simulate SiPM signals with $\tau_{\text{rise}} \approx 3 \text{ ns}$ and $\tau_{\text{fall}} \approx 50 \text{ ns}$ and then input them to the designed preamplifiers. We used the Tektronix MDO3024 oscilloscope to fetch the waveforms of the input and output signals of the preamplifier, as shown in Fig. 3(b). The output signals without the PZC have nearly the same τ_{rise} and τ_{fall} as those of the input signals. The signals after the PZC without the two-stage amplifier are $\tau_{\text{rise}} \approx 1.2 \text{ ns}$ and $\tau_{\text{fall}} \approx 20 \text{ ns}$, which are significantly improved; however, their amplitudes are reduced. Compared to these signals, the signals from the preamplifier with the two-stage amplifier after the PZC have nearly the same τ_{rise} and τ_{fall} , and their amplitudes are significantly larger. The improvement of τ_{rise} is significantly useful for a good time resolution, and a short τ_{fall} is important for avoiding the pile-up in a detector operation.

Another test was conducted to study the effect of PZC on the pile-up. We used the ps-level laser MDL-PS-450 [26] as the light source, and tuned its frequency from 0.8 MHz to the maximum 20 MHz . Photons from the laser are detected by two SiPMs, which are connected in parallel to the preamplifiers with or without the PZC. Figure 3(c) presents the signals displayed on the oscilloscope. The τ_{fall} of signal from the preamplifier without the PZC is approximately 200 ns , and a pile-up appears when the laser operates at a frequency of approximately 2 MHz . When the PZC is implemented in the preamplifier, the τ_{fall} reduces to approximately 5 ns , and there

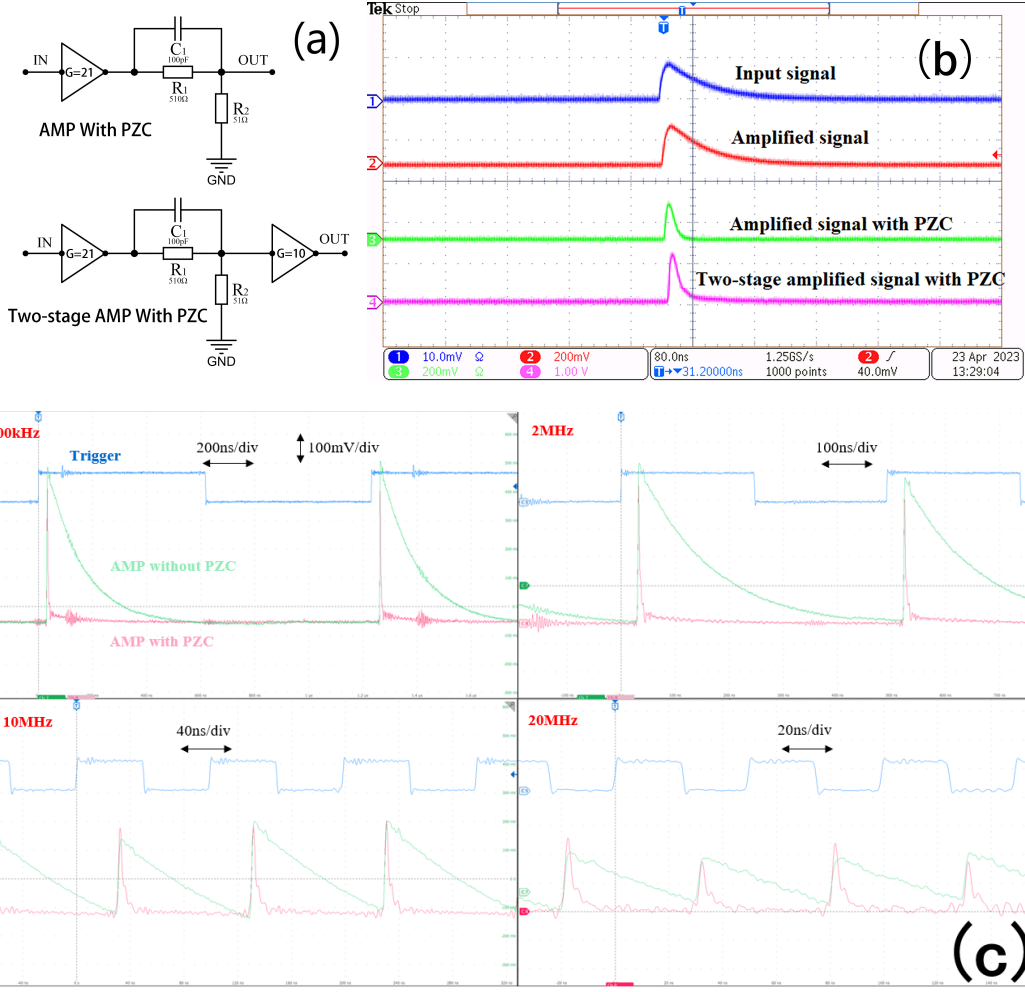


Fig. 3. PZC implementation in the preamplifier and its effects on the signal shape and pile-up. Plot (a) presents the circuit of a one-stage or two-stage amplifier with the PZC, and plot (b) presents how the τ_{rise} and τ_{fall} of the signals improved by the PZC in laboratory testing. Plot (c) presents the SiPM signals from a preamplifier with or without the PZC and are displayed on an oscilloscope in testing with photons from a pulsed laser [26], which operates at a frequency between 0.8 MHz–20 MHz.

is no pile-up even when the laser is operating at a frequency of 20 MHz. This testing indicates that the PZC significantly reduces the pile-up in a high signal rate environment.

III. PERFORMANCE OF THE PREAMPLIFIER

To apply this preamplifier in experiments, such as the possible upgraded KLM in Belle II, we studied the performance characteristics of the preamplifier, including the stability of the gain, dynamic of the output signal, noise level, and measurement of a single photoelectron signal. Based on the performance, we then combined the preamplifier with the SiPM and studied their time resolutions.

A. Linearity between input and output signals

We set $R_f = 1 \text{ k}\Omega$ and $R_g = 50 \Omega$, as shown in Fig. 2, and calculated the gain of the preamplifier to be +21 V/V. We used DT5810B [25] to generate SiPM-like pulses with $\tau_{\text{rise}} = 1 \text{ ns}$ and $\tau_{\text{fall}} = 50 \text{ ns}$, and amplitudes ranging from 2 mV–80 mV as the input signals to the preamplifier; the Tektronix MSO58 oscilloscope was then used to measure the output signals to study the linearity of the preamplifier. An ideal and stable Gaussian distribution of the gains was obtained from these tests. Fitting the distribution with a Gaussian function yields a mean of 21 and $\sigma = 0.087 \pm 0.002$, which demonstrates a good stability of the gain. To study the dynamics range of the preamplifier, the amplitudes of the input signals were extended from 80 mV to 200 mV. A good linear relationship was demonstrated between the input signals from the generator and output signals from the amplifier in a wide dynamic range. When the supply voltage (V_{bias}) on the preamplifier increases from 2.5 V to 3.9 V, the maximum

amplitude of the input signal can be increased from 90 mV to 170 mV for the preamplifier to maintain the linearity of the gain, and the amplitude of the corresponding output signal increases from 0.9 V to 1.7 V. The gain of ~ 10 in these tests is owing to the impedance of $50\ \Omega$ in the oscilloscope. The full bandwidth and input impedance were set as 2 GHz and $50\ \Omega$ in the oscilloscope for these tests, respectively.

B. Noise level of the baseline

According to Eq. (2), the time resolution highly depends on the noise level of the output signal from the preamplifier, which mainly depends on the preamplifier baseline and the noise from the SiPM. The MSO58 oscilloscope was used with the sample rate setting as 2 GHz to measure the baseline in a time interval of 3000 ns, and the amplitudes were projected on a one-dimensional histogram. The distribution was fit with a Gaussian function and σ was obtained as the noise level of the baseline. The noise level of the preamplifier baseline measured without the SiPM was $\sigma = 302\ \mu\text{V}$. In this measurement, the input impedance of the oscilloscope was $50\ \Omega$, thus the real noise level of the preamplifier should be $\sigma_{\text{noise}} = 604\ \mu\text{V}$, which is consistent with the results of our calculation and simulation. We also measured the baseline noise levels of the preamplifier coupled to different types of SiPMs from the NDL(Beijing) Company [27, 28] and the Hamamatsu Company [24, 29], as listed in Table 1. These noise levels included noise from the SiPMs, and should be counted in the effect for the time resolution, as described in Eq. (2). As previously indicated, the noise levels shown in Table 1 are half of the real levels owing to the $50\ \Omega$ input impedance of the oscilloscope. Generally, the baseline noise level increases as the terminal capacitance and N_{pixel} increase. For a large SiPM, N_{pixel} can be at the 10^4 level and the dark count rate can be at the MHz level, thus the baseline noise level is relatively high.

C. Measurement of a single photoelectron

A typical measurement with the SiPM is that of a single photoelectron peak spectrum, which can be used to determine the performance of the SiPM. Based on the gain and resolution of a single photoelectron obtained from the spectrum, we can estimate the number of photoelectrons (or the number of fired SiPM pixels) in a measurement according to the pulse height of the signal. We measured the signal of a single photoelectron by combining an SiPM and the preamplifier for the basis of further measurements, such as the time resolution versus the number of photoelectrons.

First, the measurements were performed with S13360-1325CS, S13360-1350CS, and S13360-1375CS, which have a common photosensitive area of $1.3\ \text{mm} \times 1.3\ \text{mm}$ and different pixel sizes of $25\ \mu\text{m}$, $50\ \mu\text{m}$, and $75\ \mu\text{m}$ [24], respectively, as listed in Table 1. Figure 4(a) presents the pulse shapes of the single photoelectrons, for which $\tau_{\text{rise}} < 1\ \text{ns}$ and the amplitudes are higher than 10 mV. Occasionally, the

photosensitive area of the S13360-13* series was too small for photon collection in a detector. Our R&D for the KLM upgrade concludes the choice of a large SiPM and the combination of multiple SiPMs for a good time resolution, such as that of the 13360-6025PE from Hamamatsu [20] with a photosensitive area of $6.0\ \text{mm} \times 6.0\ \text{mm}$. Figure 4(b) presents an example of a single photoelectron signal from 13360-6025PE and the average of many signals, which are fetched by an oscilloscope. We obtained $\tau_{\text{rise}} \sim 3\ \text{ns}$, which is larger than that obtained in previous tests for the small SiPMs owing to the large capacitance of 13360-6025PE. For a small gain amplifier, the signal was able to obtain $\tau_{\text{rise}} \sim 2\ \text{ns}$ in our tests. All the tests were conducted under a weak light. We also established an SiPM circuit model based on LTspice for 13360-6025PE and simulated a single photoelectron signal with a preamplifier or an ideal preamplifier. The results of the simulations and those of the measured pulses were in very good agreement, as indicated in Fig. 4(b).

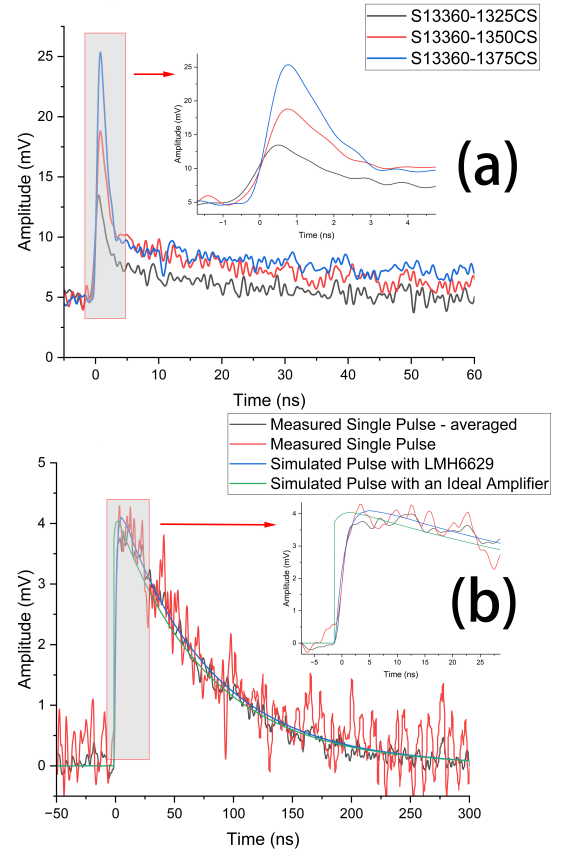


Fig. 4. Pulse shapes of single photoelectron signals from SiPMs with (a) a small photosensitive area of $1.3\ \text{mm} \times 1.3\ \text{mm}$ or (b) large area of $6.0\ \text{mm} \times 6.0\ \text{mm}$. The tests were conducted under a weak light. Plot (a) demonstrates $\tau_{\text{rise}} < 1\ \text{ns}$ and the different gains of the small SiPMs with different pixel sizes. In (b), the red curve indicates a typical single photoelectron signal and the black curve indicates the average of many signals fetched in the oscilloscope, while the blue (green) curve indicates the simulation of a single photoelectron signal from the LMH6629 (ideal) amplifier.

TABLE 1. The parameters and the baseline noise levels of different types of SiPMs. Here, N_{pixel} and C_{tot} are the number of pixels and total capacitance of an SiPM, respectively.

Model of the SiPM	Sensor area (mm ²)	Pixel size (μm^2)	N_{pixel}	C_{tot} (pF)	Baseline noise (μV)
EQR10-11-1010CS	1.0×1.0	10×10	10000	7	618
EQR10-11-3030DS	3.0×3.0	10×10	90000	31	644
EQR15-11-3030DS	3.0×3.0	15×15	40000	50	577
EQR15-11-6060DS	6.0×6.0	15×15	160000	202	1018
S13360-1325CS	1.3×1.3	25×25	2668	60	567
S13360-1350CS	1.3×1.3	50×50	667	60	500
S13360-1375CS	1.3×1.3	75×75	258	60	425
S13360-6025PE	6.0×6.0	25×25	57600	1280	750
S14160-6050HS	6.0×6.0	50×50	14331	2000	888

IV. TIME RESOLUTION ACHIEVED FROM THE COMBINATION OF THE PREAMPLIFIER AND SiPM

Time resolution is one of the most important characteristic properties of certain detectors. For a scintillation detector using SiPM as the photosensor, the time resolution is determined by the scintillator material, SiPM, and the front-end readout with the preamplifier.

To determine the time resolution of the preamplifier, DT5810B was used to generate pulse signals with different amplitudes, which were then input into two parallel preamplifiers. The Tektronix MSO58 oscilloscope was used to digitize and save the waveforms of the output signals, and to determine the arrival time of an output signal via the constant-ratio timing (CFD) method in an offline data analysis of the waveform. We obtained a distribution of the time difference between the signals from the two parallel preamplifiers. By fitting the distribution with a Gaussian function, we obtained the standard deviation σ and considered $\sigma/\sqrt{2}$ as the time resolution of one preamplifier. The time resolution versus the amplitude of the input signal is shown in Fig. 5. With $\tau_{\text{rise}} = 2$ ns being set for DT5810B, the time resolution of the preamplifier was approximately 20 ps for the input signals with amplitudes larger than 20 mV, or 30 – 50 ps for the small input signals with amplitudes of 5–10 mV. Figure 5(a) demonstrates that the time resolution worsens when τ_{rise} is increased. As indicated in Sect. II B, PZC can reduce the τ_{rise} , which is significantly useful for increasing the time resolution. We set $\tau_{\text{rise}} = 7.5$ ns and compared the preamplifiers with and without The PZC. Figure 5(b) presents their time resolutions versus the amplitude of the input signal. Although the amplitude of the output signal was reduced owing to the PZC, τ_{rise} improved and a better time resolution was obtained. For example, when testing with input signals having an amplitude of 20 mV, the time resolution increased from 50 ps to 25 ps with the implementation of the PZC.

We combined our preamplifier and the SiPM to determine the time resolution in photon detection. We used a ps level pulsed laser MDL-PS-450 [26] again as the light source, and the setup for testing and the time resolutions obtained are shown in Fig. 6. We used two SiPMs to detect the photons from the laser; these two SiPMs were connected to two preamplifiers, as shown in Fig. 6(a). We measured the amplitude and arrival time of the signals from the two detecting

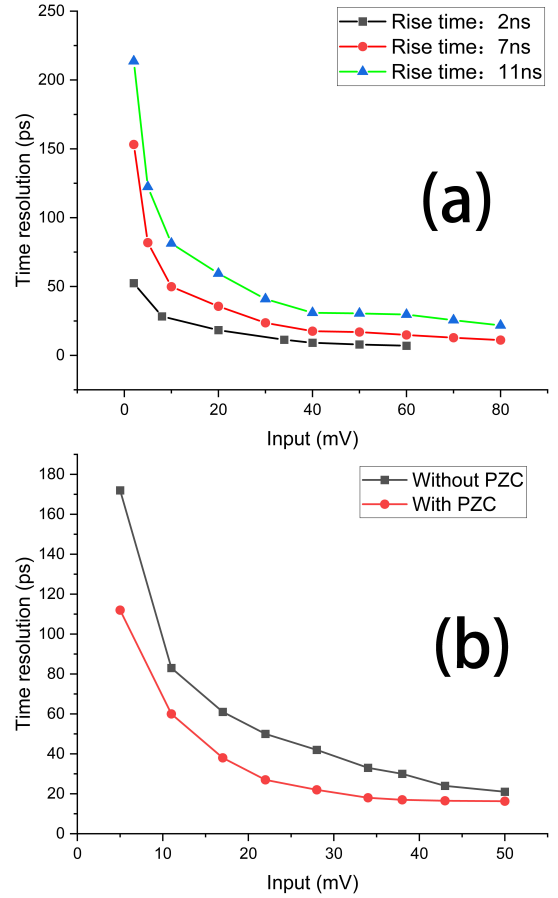


Fig. 5. The time resolution versus the amplitude of the input signals (a) at different τ_{rise} values of the input signals, or (b) with and without the PZC, for a comparison. The PZC is not applied for the measurements shown in (a), and the value of τ_{rise} of the input signals in (b) is 7.5 ns.

channels, and then determined the time resolution according to the distribution of their time difference. Typically, the time resolution highly depends on the number of detected photons. According to the amplitude of the measured signal and that of a single photoelectron signal described in Sect. III C, we can estimate the number of photons detected in the SiPM (the number of the fired pixels). We studied the time reso-

lution with small SiPMs, such as the EQR10-11-1010 from NDL (Beijing) and the S13360-1350 from Hamamatsu, and found that they have nearly the same performance, as shown in Fig. 6(b). When approximately five photons were detected, their time resolutions were between 40 – 50 ps. As the number of detected photons increased to > 40 , the time resolution was approximately 25 ps. We also studied the time resolution with large SiPMs, such as the EQR15-11-6060 from NDL and the S14160-6050 from Hamamatsu [29], both of which have a photosensitive area of $6.0 \text{ mm} \times 6.0 \text{ mm}$. When the number of photons was larger than 60, the performances of the two SiPMs were similar, and their time resolutions were better than 25 ps, as shown in Fig. 6(b). When a small number of photons were detected, S14160-6050 demonstrated a better performance than EQR15-11-6060, which is owing to its advantages of a significantly lower dark count rate and higher gain.

V. COMPARISON WITH SOME COMMERCIAL PREAMPLIFIERS

We compared this preamplifier with other commercial preamplifiers for the SiPM, such as the Hamamatsu C12332-02 [13], NDL AMP-20-2 [14], and Cremat CR-Z-SiPM [15].

1. The commercial preamplifiers are one- or two-channel devices with a size of approximately 5 cm, 10 cm, or 15 cm, whereas the array of the eight preamplifiers shown in Fig. 2(b) only has a length of approximately 10 cm. According to the schematic diagram shown in Fig. 2(a), we can improve the design for significantly higher integration in the implementation of hundreds or thousands of SiPM channels in a large detector.
2. According to the data manuals, C12332-02 has a bandwidth of 200 MHz at a gain of -20 V/V , and AMP-20-2 has a bandwidth of 350 MHz at a gain of -10 V/V . The testing demonstrates that our preamplifier has a bandwidth of approximately 426 MHz. The CR-Z-SiPM is a charge-sensitive preamplifier, which is not suitable for the amplification of a fast signal.
3. Our preamplifier has an advantage in the noise level. The testing demonstrates that its baseline noise level is approximately 0.6 mV, which is nearly 80% of that of AMP-20-2.
4. Figure 5 presents significantly good time resolutions of our preamplifier.

5. The C12332-02 of Hamamatsu uses OPA846 as the core amplifier. The LMH6629 we used for the preamplifier demonstrates a better performance considering the bandwidth, slew rate, and noise level.

6. The cost of our preamplifier per channel is approximately two orders lower than those of commercial products.

Note, the design of this preamplifier is to enable the implementation of tens of thousands of SiPM channels in a sub-detector of the possible Belle II upgrade project or the CEPC experiment in the future; these detector channels should demonstrate a very good performance. Therefore, we focus on a simple design, high integration, high time resolution, large bandwidth, large dynamic range, low noise level, and low cost.

VI. SUMMARY

Considering the R&D for the upgrade of the KLM in Belle II and the muon detector of CEPC, we designed a compact high-speed and low-noise preamplifier for the SiPM. The preamplifier has a bandwidth of 426 MHz, baseline noise level of 0.6 mV, total noise levels of less than 1 mV for the combination with different SiPMs, a large dynamic range for an input signal of up to 170 mV, and a very fast τ_{rise} for good time resolution. The PZC was found to be significantly useful for improving both the τ_{rise} and τ_{fall} of a SiPM signal, which can significantly improve the time resolution and reduce the pile-up when using a large SiPM or an array of SiPMs. A time resolution of better than 20 ps can be achieved from the preamplifier. The combinations of the preamplifier and different SiPMs demonstrated time resolutions of better than 50 ps; when the number of photons is large, a time resolution of 25 ps can be achieved. The good performance of the preamplifier is helpful for upgrading the KLM in Belle II for a new function of measuring the hit time of a neutral hadron, such as K_L^0 or a neutron, according to the hadronic cluster in the detector.

ACKNOWLEDGMENTS

We would like to thank Dr. Qi-Bin Zheng from the University of Shanghai for the Science and Technology and Prof. Gary Varner from the University of Hawai'i for the helpful discussions.

-
- [1] Y. Yang, P. C. Yang, J. Xin et al., Performance of a plastic scintillation fiber dosimeter based on different photoelectric devices. Nucl. Sci. Tech. **32**, 120 (2021). doi:10.1007/S41365-021-00965-0.
 - [2] M. Li, Z. M. Wang, C. M. Liu et al., Performance of compact plastic scintillator strips with wavelength shifting fibers using a

photomultiplier tube or silicon photomultiplier readout. Nucl. Sci. Tech. **34**, 31 (2023). doi:10.1007/s41365-023-01175-6.

- [3] T. Abe, I. Adachi, K. Adamczyk et al., The Belle II Technical Design Report, KEK Report 2010-1, 2010, arXiv:1011.0352v1. doi:10.48550/arXiv.1011.0352.

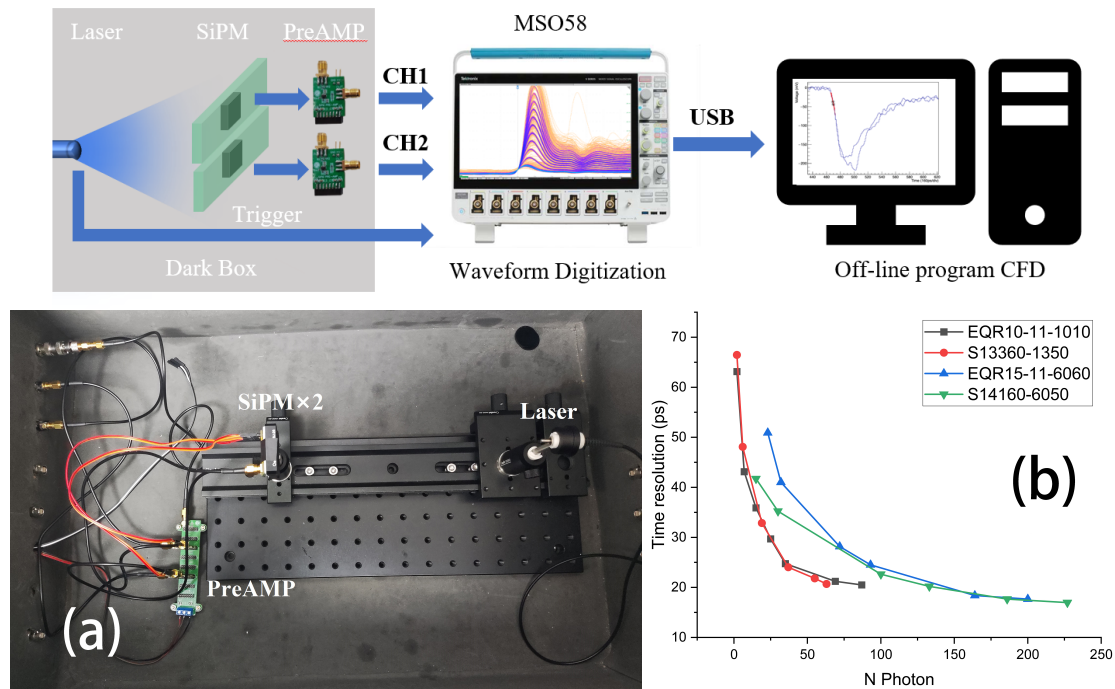


Fig. 6. Measurement of the time resolution of the preamplifier and the SiPM in photon detection. The top presents the diagram of the setup for the measurement, and (a) the bottom presents the image of the setup containing the laser, including the SiPMs and the preamplifiers in a dark box. Plot (b) at the bottom presents the measured time resolution versus the number of detected photons using various SiPMs.

- [4] I. Adachi, T. Browder, P. Krizán et al., Detectors for extreme luminosity: Belle II. Nucl. Instrum. Methods A **907**, 46 (2018). doi:10.1016/j.nima.2018.03.068.
- [5] T. Aushev, D. Besson, K. Chilikin et al., A scintillator based endcap K_L^0 and muon detector for the Belle II experiment. Nucl. Instrum. Methods A **789**, 134 (2015). doi:10.1016/j.nima.2015.03.060
- [6] F. Forti (for Belle II Collaboration), Snowmass Whitepaper: The Belle II Detector Upgrade Program, arXiv:2203.11349v1. doi:10.48550/arXiv.2203.11349.
- [7] The CEPC Study Group, CEPC Conceptual Design Report: Volume 1 - Accelerator. arXiv:1809.00285v1. doi:10.48550/arXiv.1809.00285.
- [8] The CEPC Study Group, CEPC Conceptual Design Report: Volume 2 - Physics & Detector. arXiv:1811.10545v1. doi:10.48550/arXiv.1809.00285.
- [9] V. Golovin and V. Saveliev, Novel type of avalanche photodetector with Geiger mode operation. Nucl. Instrum. Methods A **518**, 560 (2004). doi:10.1016/j.nima.2003.11.085.
- [10] Q. Y. Wei, T. P. Xu, T. T. Dai et al., Development of a compact DOI-TOF detector module for high-performance PET systems. Nucl. Sci. Tech. **28**, 43 (2017). doi:10.1007/S41365-021-00965-0.
- [11] Y. Li, C. Shen, Z. Zhang et al., Production and quality control of NICA-MPD shashlik electromagnetic calorimeter in Tsinghua University. J. Instrum. **17**, 04 (2022). doi:10.1088/1748-0221/17/04/T04005
- [12] Q. Yu, B. Tang, C. Huang et al., A prototype of the SiPM readout scintillator neutron detector for the engineering material diffractometer of CSNS. Nucl. Eng. Technol. **54**, 3 (2022). doi:10.1016/J.NET.2021.09.014.
- [13] Hamamatsu Photonics. C12332-02 Datasheet. https://www.hamamatsu.com.cn/content/dam/hamamatsu-photonics/sites/documents/99_SALES_LIBRARY/ssd/c12332-02_kacc1287e.pdf [Accessed 11 May 2023].
- [14] NDL-SiPM. AMP-20-2 Datasheet. <http://www.ndl-sipm.net/PDF/Datasheet-Preamplifier.pdf> [Accessed 11 May 2023].
- [15] Cremat. CR-Z-SiPM Datasheet. <https://www.cremat.com/CR-Z-SiPM.pdf> [Accessed 11 May 2023].
- [16] F. Corsi, A. Dragone, C. Marzocca et al., Modelling a silicon photomultiplier (SiPM) as a signal source for optimum front-end design. Nucl. Instrum. Methods A **572**, 416 (2007). doi:10.1016/j.nima.2006.10.219.
- [17] S. Seifert, H. T. van Dam, J. Huizenga et al., Simulation of Silicon Photomultiplier Signals. IEEE Trans. Nucl. Sci. **56**, 3726 (2009). doi:10.1109/tns.2009.2030728.
- [18] A. K. Jha, H. T. van Dam, M.A. Kupinski et al., Simulating Silicon Photomultiplier Response to Scintillation Light. IEEE Trans. Nucl. Sci. **60**, 336 (2013). doi:10.1109/TNS.2012.2234135.
- [19] Analog Devices. LTSpice [Online] <https://www.analog.com/en/design-center/design-tools-and-calculators/ltspice-simulator.html> [Accessed 11 May 2023].
- [20] T. Bretz, T. Hebbeker, J. Kemp, Extending the dynamic range of SiPMs by understanding their non-linear behavior. arXiv:2010.14886.
- [21] D. Sánchez, S. Gómez, J. Fernández-Tenllado et al., Multimodal simulation of large area silicon photomultipliers for time resolution optimization. Nucl. Instrum. Methods A **1001**, 165247 (2021). doi:10.1016/J.NIMA.2021.165247.

- [22] Texas Instruments. LMH6629 Datasheet. <https://www.ti.com.cn/cn/lit/ds/symlink/lmh6629.pdf>. [Accessed 11 May 2023].
- [23] J. W. Cates, S. Gundacker, E. Auffray, et al., Improved single photon time resolution for analog SiPMs with front end readout that reduces influence of electronic noise. *Phys. Med. Biol.* **63**, 18 (2018). doi:10.1088/1361-6560/aadbcd.
- [24] Hamamatsu Photonics. S13360 Datasheet. https://www.hamamatsu.com.cn/content/dam/hamamatsu-photonics/sites/documents/99_SALES_LIBRARY/ssd/s13360_series_kapton_led.pdf. [Accessed 11 May 2023].
- [25] <https://www.caen.it/products/dt5810/>. [Accessed 09 July 2023].
- [26] <http://www.cnilaser.com/PDF/MDL-PS-450.pdf>. [Accessed 09 July 2023].
- [27] Novel Device Laboratory, Beijing. EQR10 Datasheet, <http://www.ndl-sipm.net/PDF/Datasheet-EQR10.pdf>; EQR15 Datasheet, <http://www.ndl-sipm.net/PDF/Datasheet-EQR15.pdf>. [Accessed 09 July 2023].
- [28] J. Q. Jia, J. L. Jiang, K. Liang et al., EQR SiPM with P-N-P-N diode configuration. *Nucl. Sci. Tech.* **30**, 119 (2019). doi:10.1007/s41365-019-0644-9.
- [29] Hamamatsu Photonics. S14160 Datasheet. https://www.hamamatsu.com/content/dam/hamamatsu-photonics/sites/documents/99_SALES_LIBRARY/ssd/s14160_s14161_series_kapton_led.pdf. [Accessed 11 May 2023].